

Nematicity Liquid in a Trimerized-Kagome Antiferromagnet

Ichiro Tanaka and Hirokazu Tsunetsugu

The Institute for Solid State Physics, The University of Tokyo, Kashiwanoha 5-1-5, Chiba 277-8581, Japan

We theoretically study low-temperature properties of the antiferromagnetic Heisenberg model with half-integer spin S on the kagome lattice with large trimerization. We have derived a low-energy effective model for general S in terms of spin and nematicity operators in triangular units, and studied their low-temperature correlations for $S=3/2$ by classical Monte Carlo simulations. The previous study for the $S=1/2$ case [M. Ferrero *et al.*, Phys. Rev. B **68**, 214431 (2003)] reported a spin liquid state at low temperatures driven by a glassy behavior of isolated dimers and trimers of nematicities. The results for $S=3/2$ show that nematicity dimers and trimers are connected by weak links to form a defective planar network. At very low temperatures, nematicities show glassy slow dynamics, and cluster spins continue to fluctuate in a nonperiodically frozen background of nematicities. The characteristic time of glassy dynamics scales with temperature following a power law.

Heisenberg antiferromagnets on the kagome lattice is the representative frustrated spin system, and the possibility of quantum spin liquid ground state has been intensively studied for many decades both theoretically and experimentally, but its conclusion remains under debate.^{1,2)} For its better understanding, it is useful to study a related system with frustration more tamed, and we study in this letter the model on a trimerized kagome lattice, which is also called breathing kagome. This system is also interesting in itself due to a few instances of its realization. The vanadate $(\text{NH}_4)_2[\text{C}_7\text{H}_{14}\text{N}][\text{V}_7\text{O}_6\text{F}_{18}]$ (DQVOF) has a trimerized kagome network of V^{4+} ions with spin $S=1/2$, and a spin liquid behavior is observed.^{3,4)} There is also a proposal of an optical lattice with trimerized kagome geometry.⁵⁾ Recently, Ishii *et al.* synthesized $\text{Li}_2\text{Cr}_3\text{SbO}_8$, in which Cr^{3+} ions with $S=3/2$ form a trimerized kagome network, and observed a $\sqrt{3}\times\sqrt{3}$ magnetic order and plateaus in its magnetization curve.^{6,7)} A few theoretical studies discussed that its ground state is a spin liquid.^{5,8–10)}

One of the authors studied the Heisenberg antiferromagnets on a breathing pyrochlore lattice.^{11,12)} An important difference from kagome lattices lies in the parity of the number of spins in unit cell. Since the pyrochlore lattice has a tetrahedron unit, the parity is even. Its ground states have degeneracy $2S+1$, and they are all spin-singlet irrespective of spin S . By contrast, the parity is odd for the kagome lattice. For integer S , each triangular unit has a unique ground state. Therefore the ground state of the whole system is a valence bond crystal, and no symmetry is broken. The case of half-integer S is interesting and the ground state in each unit has degeneracy $4=2\times 2$, i.e. two spin doublets.¹⁴⁾ This additional nonmagnetic 2-fold degrees of freedom is related to the point group symmetry and let us call it *nematicity*, which will be explained more explicitly later. The issue to study is to see how these cluster spins and nematicities in the triangular units develop correlations at low temperatures. Ferrero *et al.* investigated this problem for the $S=1/2$ case.⁸⁾ Performing classical Monte Carlo (MC) simulations for its low-energy Hamiltonian, they observed a glassy behavior of nematicity at very low temperatures. Note that they used the term “*chirality*”, which is synonymous with our nematicity. In this letter, we will study how the low temperature physics changes for higher S . We will

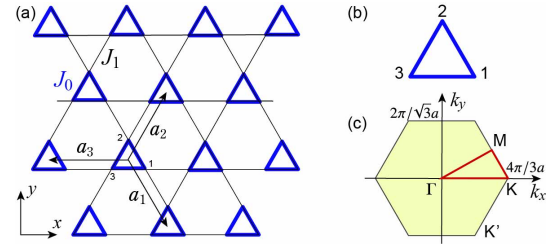


Fig. 1. (Color online) (a) Trimerized kagome lattice, aka breathing kagome. With lattice constant a , $\mathbf{a}_1=a(1/2, -\sqrt{3}/2)$, $\mathbf{a}_2=a(1/2, \sqrt{3}/2)$, and $\mathbf{a}_3=-\mathbf{a}_1-\mathbf{a}_2$. (b) Sublattice indices in unit cell. (c) Brillouin zone.

construct an effective Hamiltonian for general half integer S and perform classical MC simulations.

The model to study is the trimerized-kagome antiferromagnetic Heisenberg (TKAFH) Hamiltonian with half-integer spin S

$$\tilde{H} = J_0 \sum_{\mathbf{R}} \sum_{1 \leq i < j \leq 3} \mathbf{S}_i(\mathbf{R}) \cdot \mathbf{S}_j(\mathbf{R}) + J_1 \sum_{\mathbf{R}} \sum_{j=1}^3 \mathbf{S}_j(\mathbf{R}) \cdot \mathbf{S}_{j+1}(\mathbf{R} + \mathbf{a}_j), \quad (1)$$

where J_0 and J_1 denote the nearest-neighbor exchanges in triangles pointing up and down respectively as shown in Fig. 1(a). We will consider the case of strong trimerization $0 < J_1 \ll J_0$ in this letter. In the following, let us call up-pointing triangles *clusters*. The sum on \mathbf{R} is taken over clusters, which constitute a triangular lattice with the lattice vectors \mathbf{a}_1 and \mathbf{a}_2 . $\mathbf{S}_j(\mathbf{R})$ denotes the spin on the sublattice j shown in Fig. 1(b) with the convention $\mathbf{S}_{j+3}(\mathbf{R}) = \mathbf{S}_j(\mathbf{R})$, and define the cluster spin by $\mathbf{S}(\mathbf{R}) \equiv \mathbf{S}_1(\mathbf{R}) + \mathbf{S}_2(\mathbf{R}) + \mathbf{S}_3(\mathbf{R})$.

In the decoupled limit $J=0$, the ground state is a direct product of cluster ground states. Each cluster has 4-fold degenerate ground states $|\Phi^p(M)\rangle$, ($p=\pm$, $M=\pm 1/2$), for any half-integer spin S . They are spin doublet with $S^z=M$, and eigenstates of $(\mathbf{S}_1 + \mathbf{S}_3)^2$ with eigenvalue $(S+p/2)(S+p/2+1)$. This doublet $|\Phi^\pm\rangle$ constitutes a basis of E-irreducible representation of the C_{3v} point group of the triangular unit, and therefore describes breaking of the lattice symmetry. For later use, it is convenient to use the chiral basis:

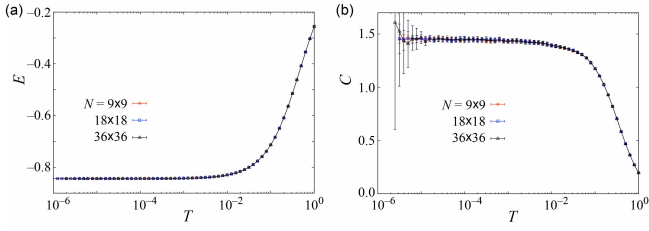


Fig. 2. (Color online) (a) Internal energy and (b) specific heat of the effective model H for $S=3/2$. Values are normalized per site, *i.e.* three spins in \tilde{H} . Error bars are estimated by the bootstrap method with 95% percentile.

$|\Phi_{L,R}(M)\rangle = 2^{-1/2}[\Phi^+(M) \pm i\Phi^-(M)]$. After lengthy calculations of Clebsh-Gordan coefficients and 6- j symbols,¹³⁾ we can represent the sublattice spin operators in terms of this chiral basis within the ground state manifold as

$$S_j(\mathbf{R}) \rightarrow \zeta S(\mathbf{R}) [\gamma + \mathbf{d}_j \cdot \boldsymbol{\tau}(\mathbf{R})], \quad \mathbf{d}_j = (\cos \omega_j, \sin \omega_j), \quad (2)$$

where $3\omega_3 = -3\omega_1 = \omega_2 = \pi$, $\zeta = (2S+1)/3$ and $\gamma = 1/(2S+1) < 1$. Note that while $S_j(\mathbf{R})$ are spin- S operators, the cluster ones $S(\mathbf{R})$ are spin-1/2. $\boldsymbol{\tau} = (\tau_1, \tau_2)$ are Pauli matrices operating in the chiral space (Φ_L, Φ_R) at each unit \mathbf{R} . These operators constitute a basis set of E-irreducible representation of the triangular point group, and describe breaking of this symmetry. Therefore, we will call them *nematicity* in this letter. Note that the chirality is represented by the other operator $\tau_3 = i\tau_2\tau_1$.¹¹⁾

The low-energy effective Hamiltonian of this system is derived by projecting \tilde{H} into the macroscopically degenerate ground states of the J_0 term. Dropping a constant term, it is the J_1 term represented with the projected operators (2)

$$H = J \sum_{\mathbf{R}} \sum_{j=1}^3 S(\mathbf{R}) \cdot S(\mathbf{R} + \mathbf{a}_j) \Gamma(\mathbf{R}, \mathbf{R} + \mathbf{a}_j), \quad (J = \zeta^2 J_1) \quad (3)$$

$$\Gamma(\mathbf{R}, \mathbf{R} + \mathbf{a}_j) \equiv [\gamma + \mathbf{d}_j \cdot \boldsymbol{\tau}(\mathbf{R})][\gamma + \mathbf{d}_{j+1} \cdot \boldsymbol{\tau}(\mathbf{R} + \mathbf{a}_j)]. \quad (4)$$

This effective Hamiltonian was previously obtained for the $S=1/2$ case by Mila.¹⁴⁾ It is important that the Hamiltonian does not change its form for higher S 's,¹⁵⁾ but the value of γ varies in addition to the renormalization of the energy unit J . We will show later that the change of γ qualitatively modifies the correlations of $\boldsymbol{\tau}$'s from the $S=1/2$ case. This approach is based on the first order perturbation, and justified as far as the renormalized energy scale J is small enough compared with the energy gap J_0 in the decoupling limit.

In order to examine how their correlations evolve with lowering temperature T , we have investigated the effective model H by classical MC simulations. Namely, spins $\{S(\mathbf{R})\}$ and nematicities $\{\boldsymbol{\tau}(\mathbf{R})\}$ are treated as *classical* unit vectors with 3 and 2 components, respectively. In the following, we use J as the units of energy and set $J=1$. The previous study for $S=1/2$ used a similar approximation but treated $\{\boldsymbol{\tau}(\mathbf{R})\}$ as 3-component classical vectors.⁸⁾ However, this difference does not change results qualitatively, since nematicities hardly point to the third direction at low T . Simulated systems are rhombus parts of the triangular lattice with edges parallel to \mathbf{a}_1 and \mathbf{a}_2 , and periodic boundary conditions are imposed. The number of sites N is up to 36×36 , and we use the standard Metropolis algorithm with local updates. Physical quantities are measured typically for 10^6 Monte Carlo steps (MCS) following 10^6 MCS of annealing for each temperature, and they

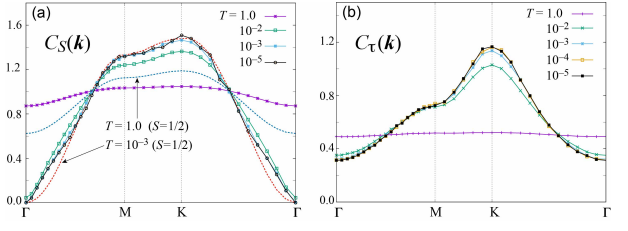


Fig. 3. (Color online) (a) Spin correlations $C_S(\mathbf{k})$ and (b) nematicity correlations $C_\tau(\mathbf{k})$ of the effective model H for $S=3/2$ and $N=36 \times 36$. For comparison, $C_S(\mathbf{k})$ for $S=1/2$ is also calculated and shown in (a).

are averaged over 128 different ensembles.

We first calculated thermodynamic quantities to check a possibility of phase transition. Since the spin part of H is isotropic, we do not expect a finite-temperature phase transition in the spin space. However, since the nematicity interactions are anisotropic, a possibility of phase transition remains. Figures 2(a) and (b) plot internal energy $E(T)$ and specific heat $C(T)$, respectively, of the effective Hamiltonian (3). The $C(T)$ curve gives no indication of diverging peak down to the very low temperature $T \sim 10^{-6}$. The internal energy provides no indication of jump either. These results imply that no phase transition occurs, neither first-order or continuous one, and the lowest-temperature state remains disordered. In contrast to the results in Ref. 8, $C(T)$ exhibits no peak, but it is common that the nearly flat part has a value ~ 1.5 , although their $\boldsymbol{\tau}$ has 3 components. We will discuss this point later.

We next investigate correlations of spins and nematicities. Two-dimensional systems with continuous internal symmetry often undergo a phase transition at $T=0$, and in such a case a related correlation function shows a divergent temperature dependence.¹⁶⁾ Define spin and nematicity correlation functions as $C_O^{\mu\nu}(\mathbf{k}) \equiv N^{-1} \sum_{\mathbf{R}, \mathbf{R}'} \langle O_\mu(\mathbf{R}) O_\nu(\mathbf{R}') \rangle e^{-i\mathbf{k} \cdot (\mathbf{R} - \mathbf{R}')}$, ($O=S, \tau$) and let $C_S(\mathbf{k}) = \sum_\mu C_S^{\mu\mu}(\mathbf{k})$ and $C_\tau(\mathbf{k})$ denote the larger eigenvalue of the latter one. Note that measured $\langle S_\mu(\mathbf{R}) S_\nu(\mathbf{R}') \rangle$ is proportional to the identity matrix within statistical errors. We have calculated $C_S(\mathbf{k})$ for all \mathbf{k} 's, and plot the results along the high symmetry axes in Fig. 3(a). It has a broad peak at the Brillouin zone corners (K and K') at all T 's, which indicates antiparallel or a 120° -type spin correlation between nearest neighbor sites. The peak does not grow or narrow with lowering temperature. This sharply contrasts with the behavior of the growing 120° structure in the antiferromagnetic Heisenberg model on the triangular lattice.^{16, 17)}

Nematicity correlation function $C_\tau(\mathbf{k})$ is plotted in the same way in Fig. 3 (b). Compared to the spin correlations, the peak at K point is more prominent. However, it remains broad and its width and height barely change at low temperatures. These results clearly demonstrate that the effective Hamiltonian (3) exhibits no tendency of long-range order in not only spin but also nematicity spaces. In this sense, the system remains in the liquid phase of spin and nematicity.

The previous study for the $S=1/2$ case pointed out that this low-temperature state has a unique character in their local nematicity correlations.⁸⁾ To quantify this, let us examine for each bond $\Gamma(\mathbf{R}, \mathbf{R} + \mathbf{a}_j)$ defined in Eq. (4), which is bounded as $\Gamma_- \leq \Gamma(\mathbf{R}, \mathbf{R}') \leq \Gamma_+$ with $\Gamma_- = -(1-\gamma^2) < 0$ and $\Gamma_+ = (1+\gamma)^2$. Each site is connected to 6 bonds, and MC snapshots for the $S=1/2$ case showed a unique imbalance in Γ among these 6 bonds.⁸⁾

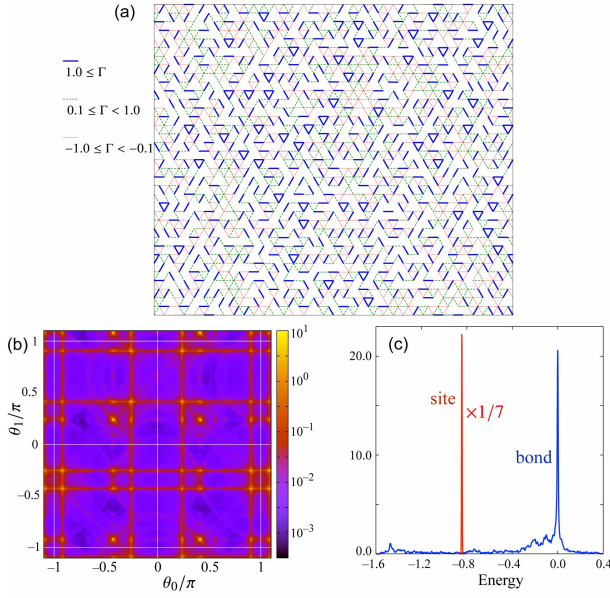


Fig. 4. (Color online) (a) Snapshot of nematicity correlations $\Gamma(\mathbf{R}, \mathbf{R}')$ for the $S=3/2$ case at $T=10^{-5}$. The system size is $N=36 \times 36$. (b) Pair distribution $P(\theta_0, \theta_1)$ calculated at $T=10^{-5}$ with averaging over 6144 ensembles. (c) Distribution function of bond and site energies for the snapshot (a). Each peak is broadened by a Gaussian with width 0.002 and 0.005 for site and bond energy, respectively.

At majority of sites, one and only one bond has a nonvanishing value $\approx \Gamma_+$, and those bonds were called *dimers*. At most of the remaining sites, τ 's form *trimers*, which are called triangles in the previous study.⁸⁾ Three sites are connected by three bonds with Γ_+ to form a triangular unit, while $\Gamma=0$ for the remaining 12 bonds.

For the $S=3/2$ case, a MC snapshot of nematicity correlations $\Gamma(\mathbf{R}, \mathbf{R}')$ is plotted in Fig. 4(a). It exhibits similarities and important differences compared with the $S=1/2$ case. Bonds with large Γ value are shown by thick blue line, and the most noticeable similarity is that most of the sites belong to a dimer or a trimer. An important difference is that many of the remaining bonds have a sizable Γ , and let us call them *weak links*. Thus, dimers and trimers are not isolated but connected by these weak links to form a *defective planar network* with modulated bond strengths mixed with small disconnected blobs such as unglued dimers and hexamers.

Spins fluctuate on this network with modulated effective exchange couplings $\{\Gamma(\mathbf{R}, \mathbf{R}')\}$, which are predominantly antiferromagnetic. Since the network extends over the whole system, spins establish long-range correlations, and this is manifested by $C_S(\mathbf{k}) \sim |\mathbf{k}|$ around Γ point as shown in Fig. 3(a). This nonanalyticity indicates a power-law scaling of long-range asymptotics in envelope $|\langle \mathbf{S}(\mathbf{R}) \cdot \mathbf{S}(\mathbf{0}) \rangle| \sim \Lambda^{1/2} R^{-5/2}$, where Λ is the wavenumber cutoff. By contrast, the $S=1/2$ result is smooth, $C_S(\mathbf{k}) \sim k^2$, and this is a consequence of short-range spin correlations confined within isolated dimers and trimers.

Let us investigate the origin of these local nematicity correlations at low T . Local energy (3) is a product of $\mathbf{S} \cdot \mathbf{S}'$ and Γ . Thus lowering energy requires either $\mathbf{S} \cdot \mathbf{S}' \sim +1$ and $\Gamma \sim \Gamma_-$, or $\mathbf{S} \cdot \mathbf{S}' \sim -1$ and $\Gamma \sim \Gamma_+$, and the latter is more effective since $|\Gamma_-| < \Gamma_+$. Therefore, many bonds realize $\Gamma(\mathbf{R}, \mathbf{R}+\mathbf{a}_j) \sim \Gamma_+$ and this requires $\boldsymbol{\tau}(\mathbf{R}) \approx \mathbf{d}_j$ and $\boldsymbol{\tau}(\mathbf{R}+\mathbf{a}_j) \approx \mathbf{d}_{j+1}$. This con-

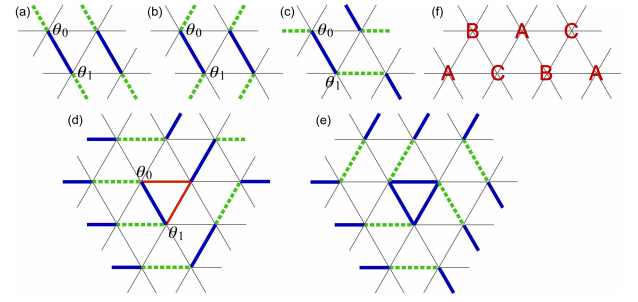


Fig. 5. (Color online) Nematicity correlations in some degenerate ground states: $(\delta\theta_0, \delta\theta_1) =$ (a) $(+\Delta, -\Delta)$, (b) $(+\Delta, +\Delta)$, (c) $(-\Delta, -\Delta)$, (d) $(-\Delta, +\Delta)$. (e) Mixed with a trimer. (f) Three-sublattice structure. In (a)-(e), strong bonds with Γ_s are shown by blue solid line, while weak links with Γ_w by green dotted line. While the configurations (a)-(c) are periodic, (d) is a local realization including bonds with $\Gamma = -(3/4)^2$ shown in red.

strains Γ on the other bonds connected to the site \mathbf{R} or $\mathbf{R}+\mathbf{a}_j$. This is because $\boldsymbol{\tau}(\mathbf{R}) \cdot \mathbf{d}_{j\pm 1} \approx -1/2$ and this enforces $\Gamma(\mathbf{R}, \mathbf{R}+\mathbf{a}_{j\pm 1}) \sim (\gamma-1/2)^2$, i.e. 0 for $S=1/2$. This explains the configuration of isolated nematicity dimers in the $S=1/2$ case.⁸⁾ The same argument predicts for our $S=3/2$ case that nematicity dimers are weakly connected by all the other bonds with $\Gamma \sim 1/16$, but the observed snapshot exhibits different correlations. This is clearly seen in the distribution function Fig. 4(b) of angle pairs $P(\theta_0, \theta_1)$, where θ_0 and θ_1 are the angle of $\boldsymbol{\tau}(\mathbf{R})$ and $\boldsymbol{\tau}(\mathbf{R}+\mathbf{a}_1)$, respectively. The above argument predicts a sharp peak at $(\theta_0, \theta_1) = (\omega_1, \omega_2) = (-\pi/3, \pi)$. However, the calculated results show that the peak splits with a finite deviation. We will continue analysis to clarify this point.

To obtain the lowest-energy configuration of spins and nematicities for the $S=3/2$ case, we have performed numerical annealing using a rhombus part with $N=6 \times 6$. The initial configuration is the one where nematicity dimers are periodically aligned with $(\theta_0^{(0)}, \theta_1^{(0)}) = (-\pi/3, \pi)$ and a random configuration is set for spins. The annealed result is again a periodic pattern with $(\theta_0^*, \theta_1^*) = (\theta_0^{(0)}, \theta_1^{(0)}) + (\delta\theta_0, \delta\theta_1)$ shown in Fig. 5(a), but the bonds shown by thin line have $\Gamma=0$ within numerical accuracy. This means that $\delta\theta_0 = -\delta\theta_1 = \Delta$ with $\Delta = \cos^{-1} \gamma - \pi/3 \approx 0.0862\pi$, and this leads to $\Gamma_s = (3\phi/4)^2 \approx 1.4726$ for dimer and $\Gamma_w = (3/4\phi)^2 \approx 0.2149$ for weak link, where $\phi = (\sqrt{5}+1)/2$ is the golden ratio. Spin configuration is Néel like along each chain of coupled dimers, but has no correlation between different chains. The corresponding energy is $E_0^* = -27/32 = -0.84375$ per site. The lowest-energy configuration is degenerate, even within periodic ones. Figure 5 (b) and (c) show some of them with a doubled unit cell, and the weak links are now along \mathbf{a}_2 and \mathbf{a}_3 .

These straight chains of weakly connected dimers do not exhaust the degeneracy of the lowest-energy configuration. First, these chains can bend with no energy cost. Another variant is the one shown in Fig. 5(d) in which weak links connect differently with $\Gamma < 0$. Secondly, one can mix a trimer and it changes the direction of dimers as shown in Fig. 5 (e). Thirdly, there also exist two-dimensional configurations, and a typical example is a 120° state shown in Fig. 5(f). This is a state with three sublattices A-C, where cluster spins and nematicities exhibit an ordinary 120° order with $\theta_A - \theta_B \equiv \theta_B - \theta_C \equiv 2\pi/3$ modulo 2π , and this state has a continuous degeneracy in both spaces.

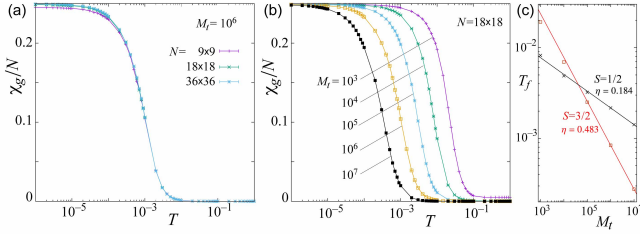


Fig. 6. (Color online) Semi-log plot of glass susceptibility of nematicities. (a) System size dependence. (b) Dependence on M_t . Data for $M_t=10^6$ are a different set from that in (a). (c) Scaling of the freezing temperature T_f defined by the midpoint of each slope in (b).

Thus, the lowest-energy configuration has very large degrees of freedom, supposedly a macroscopic entropy as for the $S=1/2$ case,¹⁴⁾ but we leave its estimate for a future study. The snapshot in Fig. 4(a) is one example. We plot in Fig. 4(c) the integrated distribution of bond and site energies in this snapshot. Site energy is defined as half of the sum of the related 6 bond energies. Bond energies have a large variance and range from -1.5601 to 0.3883 . Many of them are around zero, which means energetically disconnected bonds, i.e., missing bonds in the defective network. In contrast, site energies have only a small variance, and its maximum and minimum differ by only 0.0125 . Its average value is $\bar{E}_{\text{site}} = -0.84374$, almost identical to E_0^* considering the effect of nonzero temperature.

Now, let us come back to the discussion of the low- T value of C . Since \mathbf{S} and $\boldsymbol{\tau}$ are both classical unit vectors, Dulong-Petit law predicts that each of their angles contributes $1/2$ to C , and this explains the value ~ 1.5 in Fig. 2(b). By contrast, for $S=1/2$, $C=3/2$ was found in Ref. 8 using 3-component $\boldsymbol{\tau}$, and our calculation using 2-component $\boldsymbol{\tau}$ found $C=1$. In both cases, $1/2$ is missing and this is because half the spin degrees of freedom are zero modes in dimers and trimers.⁸⁾ The value in Fig. 2(b) is slightly smaller than $3/2$, and this reduction is also due to spin zero modes in disconnected blobs mixed in the defective network. Precise counting of zero modes requires analysis of density and shapes of isolated blobs together with analysis of local spin structure in each blob. This is another challenge to be studied in future.

Lastly, let us discuss the glassy behavior of nematicities, which was reported for the $S=1/2$ case,⁸⁾ while spin glass behaviors in undistorted kagome has been discussed much longer.¹⁸⁾ At very low T , a crossover takes place into a state where nematicities are frozen and only spin degrees of freedom fluctuate subject to the frozen pattern of effective exchange couplings.^{8,19,20)} This crossover is signaled by the nematicity glass susceptibility

$$\chi_g \equiv \frac{1}{N} \sum_{\mathbf{R}, \mathbf{R}'} \left[\frac{1}{M_t} \sum_{t=1}^{M_t} \boldsymbol{\tau}_t(\mathbf{R}) \cdot \boldsymbol{\tau}_t(\mathbf{R}') \right]^2 \quad (5)$$

where $\boldsymbol{\tau}_t(\mathbf{R})$ is the variable at Monte-Carlo step t . Note that χ_g takes a value of $O(N)$ in states where nematicities do not fluctuate with “time” t , which include both regularly ordered and glassy states. Since the possibility of regularly ordered state is already excluded by the absence of sharp peak in $C_r(\mathbf{k})$, a nonvanishing value of χ_g/N means a glassy behavior of nematicity. Figure 6 shows its temperature dependence for various values of system size and M_t . Panel (a) shows that χ_g/N

grows noticeably at $T \lesssim 10^{-3}$, and this is an evidence of *freezing* to a glassy state. The system size dependence is very small except in the region of lowest temperatures, and the value increases with N there. This indicates that this glassy behavior survives in the $N=\infty$ limit, but it is premature to conclude this.

Figure 6(b) shows the results with varying measurement time M_t . With increasing M_t , freezing starts at a lower temperature, and this agrees with the previous study for the $S=1/2$ case.⁸⁾ Each time multiplying M_t by the factor 10, the whole curve moves with a nearly constant shift towards the lower-temperature side in this semi-log plot. This implies the characteristic freezing temperature scales as $T_f \sim M_t^{-\eta}$, and the exponent is estimated in Fig. 6(c) as $\eta \approx 0.483$. Therefore, the defective network of nematicity has slow Monte Carlo dynamics, and its time scale t_f grows with lowering temperature as $t_f \sim T^{-1/\eta}$. We have also calculated the results for the $S=1/2$ case. The difference from the $S=3/2$ case is only quantitative and the exponent is smaller $\eta \approx 0.184$, while the temperature dependence was claimed activation type in the previous study.⁸⁾ This nonuniversal exponent may imply that it is only a transient behavior but this scaling holds well down to the lowest temperatures in our simulation.

In this letter, we have theoretically studied the trimerized kagome antiferromagnetic Heisenberg model with half integer spin S in the region of large trimerization. For general S , we constructed its low-energy effective Hamiltonian in terms of spin and nematicity of each triangular unit. We then performed its classical Monte Carlo simulations for the $S=3/2$ case and studied its low temperature properties. We found that nematicities form local dimers and trimers as for the $S=1/2$ case, but they are weakly coupled to form a defective planar network mixed with disconnected small blobs. Nematicities also show glassy slow Monte Carlo dynamics, and its characteristic time scale grows with temperature following a power law. Concerning spin interactions, they are modulated in space according to the pattern of defective network of nearly frozen nematicities, and many bonds are effectively broken. Spin correlations grow at low temperatures but exhibit no periodic pattern detected by a sharp peak in $C_s(\mathbf{k})$. Therefore, the low-energy state is a strongly correlated classical spin liquid on a defective network of nematicities with glassy slow dynamics. Since nematicity represents breaking of the triangular symmetry of each unit, it couples to local lattice distortion. It is worthwhile to note that one can detect these nematicities in principle by measuring E-mode of local lattice distortion.

Acknowledgment The major part of the numerical calculations were performed at the Supercomputer Center, ISSP, at the University of Tokyo.

- 1) G. Misguich and C. Lhuillier, in “*Frustrated Spin Systems*”, (ed.) H. T. Diep, (World Scientific, 2004).
- 2) P. Mendels and A. S. Wills, in “*Introduction to Frustrated Magnetism*”, (ed.) C. Lacroix, P. Mendels, and F. Mila, (Springer, 2010) and references therein.
- 3) L. Clark, L.-C. Orian, F. Bert, M.A. De Vries, F.H. Aidoudi, R.E. Morris, P. Lightfoot, J.S. Lord, M.T.F. Telling, P. Bonville, J.P. Attfield, P. Mendels, and A. Harrison, Phys. Rev. Lett. **110**, 207208 (2013).
- 4) L.-C. Orian, B. Bernu, P. Mendels, L. Clark, F.H. Aidoudi, P. Lightfoot, R.E. Morris, and F. Bert, Phys. Rev. Lett. **118**, 237203 (2017).
- 5) L. Santos, M. A. Baranov, J. I. Cirac, H.-U. Everts, H.Fehrmann, and M. Lewenstein, Phys. Rev. Lett. **93**, 030601 (2004).

- 6) K. Iida, J-PARC MLF Experimental Report, Project No. 2017A0143 (2017).
- 7) Yuto Ishii, Doctoral Thesis submitted to Hokkaido University, 2020.
- 8) M. Ferrero, F. Becca, and F. Mila, Phys. Rev. B **68**, 214431 (2003). Note that the direction of \mathbf{d} vectors differ from ours since they chose different wave function bases depending on the cluster position.
- 9) R. Schaffer, Y. Huh, K. Hwang, and Y.B. Kim, Phys. Rev. B **95**, 054410 (2017).
- 10) M. Iqbal, D. Poilblanc, and N. Schuch, Phys. Rev. B **101**, 155141 (2020).
- 11) H. Tsunetsugu, J. Phys. Soc. Jpn. **70**, 640 (2001); H. Tsunetsugu, Phys. Rev. B **65**, 024415 (2001).
- 12) H. Tsunetsugu, Prog. Theor. Exp. Phys. **2017**, 033101 (2017).
- 13) A. Messiah, *Quantum Mechanics*, Vol. II, Appendix C, (North-Holland, 1962).
- 14) F. Mila, Phys. Rev. Lett. **81**, 2356 (1998).
- 15) Reference 8 remarked that the same type of effective Hamiltonian was derived for general half integer S by M. Mambrini, but we have found no related publication.
- 16) H. Kawamura and S. Miyashita, J. Phys. Soc. Jpn. **53**, 4138 (1984).
- 17) H. Kawamura, A. Yamamoto, and T. Okubo, J. Phys. Soc. Jpn. **79**, 023701 (2010).
- 18) P. Chandra, P. Coleman, and I. Ritchey, J. de Phys. I **3**, 591 (1993).
- 19) F. Mila and D. Dean, Eur. Phys. J. B **26**, 301 (2002).
- 20) O. Cépas and B. Canals, Phys. Rev. B **86**, 024434 (2012).